The electrooxidation of small organic molecules on platinum nanoparticles supported on gold particle size vs. particle shape effect

Scheijen, F.J.E.

Award date:
2005

The Electrooxidation of small organic Molecules on Platinum Nanoparticles supported on Gold

Particle Size vs. particle Shape Effect

Graduation Report by F.J.E. Scheijen

Coaches: T.H.M. Housmans

M.T.M. Koper

Date: 05-05-2005

Published as F.J.E.Scheijen, G.L. Beltramo, S. Hoppener, T.H.M.Housmans, M.T.M.Koper, in preparation

Abstract

The electrocatalytic properties of small platinum nanoparticles were investigated for the oxidation of CO, methanol and formic acid using voltammetry, chronoamperometry and Raman spectroscopy. The particles were generated by galvanostatic deposition of platinum on a polished gold surface from an H_2PtCl_6 containing electrolyte, and ranged between a diameter of 10-20 nm for low platinum surface concentrations, 10-120 nm for medium concentrations, and full Pt monolayers for high concentrations. CO stripping and bulk CO oxidation experiments on the particles up to 120 nm in diameter displayed a pronounced "particle size effect". The CO oxidation current-time transients show a current decay for low platinum coverages and a current maximum for medium and high coverages. These results were also observed in the literature for particles of 2-5 nm size and agglomerates of these particles. The similarities in results despite large differences in particle diameter suggest that the particle morphology is more important that actual size.

Contents

1. Introduction

Particles of nanoscale diameter are of scientific interest, due to the different, often unexpected, catalytic properties compared to bulk electrode materials. Moreover, they are commonly used in technical electrodes. Therefore, understanding of their electrochemical properties is an important issue in the development of efficient fuel cell catalysts. Especially the electrocatalysis of small organic molecules such as carbon monoxide (CO), methanol (MeOH) and formic acid (HCOOH) is an interesting field of study, as these reactions play an important role in fuel cell catalysis [1, 2] and they display pronounced size-dependent catalytic properties.[3-9] Due to the fact that platinum is one of the most active dehydrogenation catalysts, Pt nanoparticles are of particular importance.

In a recent paper, Friedrich et al.[9] reported a distinct particle size dependence for the electrooxidation of carbon monoxide on colloidal platinum nanoparticles supported on polycrystalline gold. They found that the CO oxidation potential on particles with an average diameter of 3 nm is shifted to higher potentials (300-500 mV) when compared to polycrystalline platinum electrodes. When the size of the colloidal particles is increased from 3 to 10-16 nm the oxidation potential was found to decreases again. It was suggested that the origin of this "particle size effect" lies in to geometrical structure of the particles (and to a lesser extent the electronic properties).

Maillard et al. observed a similar effect for platinum nanoparticles ranging from 1 to 4 nm supported on glassy carbon (GC).[10] They ascribed the size effect to a limited mobility of CO_{ads} on particles smaller than 2 nm. They assume a particle size dependent diffusion coefficient, which is low for small particles (<2 nm) and higher for larger particles (>3 nm). Although Arenz et al.[11] also obtained similar results for Pt particles between 1 and 5 nm supported on carbon, they attributed the difference in CO oxidation potential for varying particle sizes to the number of defects present on the surface of a particle. As defects are able to dissociate water to form OH_{ads}, the higher number of defects on larger particles results in a shift of the CO oxidation peak to lower potentials.

For the oxidation of methanol, Park et al. reported a particle size dependence for carbon supported particles in the range of 2-9 nm.[8] On particles larger than 4 nm in diameter, the recorded methanol oxidation current densities were found to approach those of polycrystalline Pt electrodes. The decreasing MeOH oxidation rate for particles smaller than 4 nm was ascribed to a decrease in contiguous Pt terrace sites. This particle size dependence of the methanol oxidation reaction was also observed by Frelink et al.[6] However, they measured a more or less constant reaction rate for particles larger than 4.5 nm. Two possible explanations for the decrease in activity with decreasing particle size were given: 1) the coverage of OH_{ads} increases, thus, blocking empty sites, resulting in a decrease in the amount of COH_{ads} (an intermediate species in the methanol decomposition), or 2) smaller particles have fewer preferential adsorption sites for methanol. In addition to these findings, Cherstiouk et al.[7] observed lower methanol oxidation rates for Pt particles in the range of 1.5-3 nm compared to polycrystalline Pt,

which they ascribed to stronger poisoning of the nanoparticles as compared to polycrystalline surfaces due to slower oxidation of CO. Despite numerous attempts to explain the origins of the "particle size effect" on these electrooxidation reactions, it is still unclear whether the observed phenomena are a consequence of electronic or geometric effects.

The effect of particle size in the electrooxidation of formic acid was also investigated by Park et al.[8] In contrast to methanol, the oxidation rate of formic acid on small particles was found to be considerably higher than for larger particles. It was suggested that formic acid, unlike methanol, does not require Pt site ensembles to react to CO_2 and, thus, in combination with a lower poisoning rate, leads to higher oxidation rates. Moreover, unlike the oxidation of CO and methanol, formic acid does not need the addition of an oxygen atom (i.e. no reaction with surface oxygen containing species, like OH_{ads}, is necessary) to form carbon dioxide.

Apart from an interesting particle size effect, the three molecules discussed above are also interesting to study from the perspective of the methanol oxidation scheme. Methanol is one of the most promising fuels for a fuel cell, as it can be catalytically oxidized on a platinum surface, yielding CO_2 and six electrons per methanol molecule.

$$CH_3OH + H_2O \rightarrow CO_2 + 6H^+ + 6e^- \qquad (9.1)$$

This reaction has a favorable thermodynamic potential of 0.04 V vs. RHE and can theoretically allow fuel cell power outputs close to that of a hydrogen-based fuel cell. Unfortunately, formation of surface poisoning species and soluble intermediates, lower the overall efficiency of the fuel cell. Carbon monoxide has been identified as the primary poisoning species in many different studies,[10, 12-15] while formic acid and formaldehyde are formed as intermediate products.[16-19] The overall methanol oxidation scheme as presented by Wang et al. is shown in Fig. 1.[17, 18] It is generally accepted that the oxidation of methanol proceeds through a dual pathway, namely a direct pathway involving the formation of intermediate species such as formic acid and formaldehyde, and an indirect pathway via adsorbed CO. Again, the effects of the particle size on the selectivity and activity of the direct and indirect pathway are not

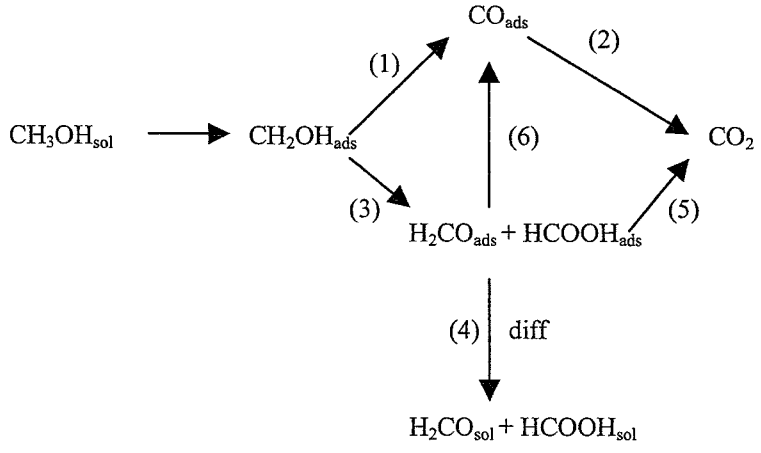

Figure 1. *Schematic representation of the parallel pathway mechanism for methanol oxidation on platinum electrodes.*

known.

From this perspective it is interesting to study the mechanism and kinetics of the oxidation reaction of these three molecules on platinum nanoparticles. The goal in this report is to gain deeper understanding of the anomalous catalytic properties of nanoparticles for the oxidation of carbon monoxide, methanol and formic acid. As CO acts as a neutral probe toward the surface reactivity and structure sensitivity, this reaction will be used as a model reaction for studying the particle size effect. The oxidation of methanol and formic acid will be discussed in light of the findings presented for CO. The Pt nanoparticles will be generated by galvanostatic deposition from a platinum containing solution on a polycrystalline gold support and characterized by cyclic voltammetry and atomic force microscopy (AFM).[9] The influence of the particle size on the catalytic activity towards oxidation of CO, MeOH and HCOOH will be investigated using cyclic voltammetry and chronoamperometry and Raman spectroscopy.

2. Experimental

All measurements were performed in a standard three-electrode cell, which was cleaned by boiling in a 1:1 mixture of concentrated sulfuric acid and nitric acid, followed by boiling twice with Milli-Q water (Millipore Milli-Q gradient A10 system, 18.2 MΩ cm, 3 ppb total organic carbon) prior to each experiment. The counter electrode consisted of a coiled platinum wire, and the reference electrode consisted of a Mercury-Mercury Sulfate Electrode (MMSE: $Hg|Hg_2SO_4|K_2SO_{4\,(sat)}$) connected via Luggin capillary.

The working electrode was a gold disk of 5 mm in diameter embedded in a Teflon sheath, which was mechanically polished with alumina (up to 0.3 μm), rinsed and treated ultrasonically in Milli-Q water before use. Prior to each experiment the electrode was cleaned by applying twenty-five potential sweep oxidation and reduction cycles from 0.055 V to 1.805 V vs. RHE at 200 $mV \cdot s^{-1}$.

The blank electrolyte consisted of 0.5 M H_2SO_4 and was prepared with concentrated sulfuric acid (Merck, "Suprapur", 96%) and Milli-Q water. The methanol and formic acid containing electrolytes consisted of the blank electrolyte and 0.1 M methanol (Merck, pro analysi, 99.8%) and 0.1 M formic acid (Merck, extra pure, 98-100%), respectively. Argon (N50) was used to deoxygenate all solutions.

The AFM used for surface characterization was a Multimode Nanoscope IIIa from Digital Instruments (DI), California. For the images a standard Si tip from Mikromasch (NSC 35, with a typical force constant of 7.5 N m^{-1}) was used in the tapping mode.

Surface-Enhanced Raman Spectroscopic (SERS) measurements were performed using a DILOR T64000 spectrograph with a holographic grating of 600 g/mm. The slit and pinhole of the system were both set at 100 μm and a CCD camera with 1024x256 pixels was used as detector. A 633 nm excitation line from a He-Ne laser was used with a power of 13 mW on the sample. The microscope objective was an Olimpus 50X, not immersed in the electrolyte. The laser spot on the electrode surface had a diameter of ~5μm. A notch filter was used to filter the Raman signal produced inside the fiber optics before reaching the sample and the excitation line after scattering from the sample. With this configuration a resolution of 1.5 cm^{-1} is obtained.

The electrode in the Raman experiments was roughened by applying a succession of potential sweep oxidation and reduction cycles in 0.1 M KCl at 500 mVs^{-1} from 1.25 V to –0.25 V vs. the Ag/AgCl electrode, with waiting times of 1.3 seconds at 1.25 V and 30 seconds at –0.25 V.[20] The electrochemical Raman cell had an optical quartz window parallel to the electrode surface. Measurements were performed at room temperature (22 °C) with a computer-controlled Autolab potentiostat (PGSTAT12). All potentials reported in the paper have been converted to the RHE scale.

3. Results and Discussion

3.1. System Cleanliness and Surface Structure

The system cleanliness and structure of the gold electrode was checked by measuring a blank cyclic voltammogram (BCV) in 0.5M H_2SO_4 at a scan rate of 20 $mV \cdot s^{-1}$. A typical voltammogram of the polished gold electrode is shown in Fig. 2. The BCV displays the characteristically low double layer charge and typical surface oxidation region, which starts at ca. 1.35V vs. RHE.

3.2. Platinum Deposition and Atomic Force Microscopy Imaging

The platinum nanoparticles were generated by galvanostatic deposition of platinum on the gold surface from a 0.02 M H_2PtCl_6 containing solution. Three surfaces with low, medium and high platinum concentrations were generated by applying a constant current and changing the deposition time. The applied current was 50 μA, while the deposition times were 5 and 40 seconds for the medium and high Pt coverage, respectively. For deposition times shorter than five seconds results become less reproducible. Therefore, the surface with the lowest platinum concentration was generated by applying a current of 5 μA for 5 seconds.

The generated surfaces were characterized by cyclic voltammetry and AFM imaging. The corresponding BCVs and AFM images are presented in Fig. 3 and 4, respectively. Fig. 3 shows that increasing the amount of platinum by increasing the deposition time results in an increase in the charge in the low potential region (between 0.05 V and 0.3 V vs. RHE), which can be ascribed to hydrogen adsorption/desorption on the deposited platinum. The features starting at 0.85 V in the positive going scan can be ascribed to oxidation of the platinum and the corresponding oxide reduction peak lies at

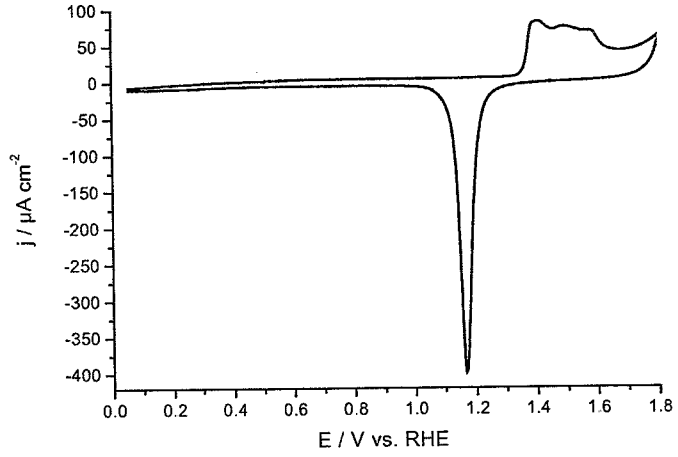

Figure 2. *Blank cyclic voltammogram of polycrystalline gold in 0.5 M H_2SO_4. The scan rate was 20 $mV \cdot s^{-1}$.*

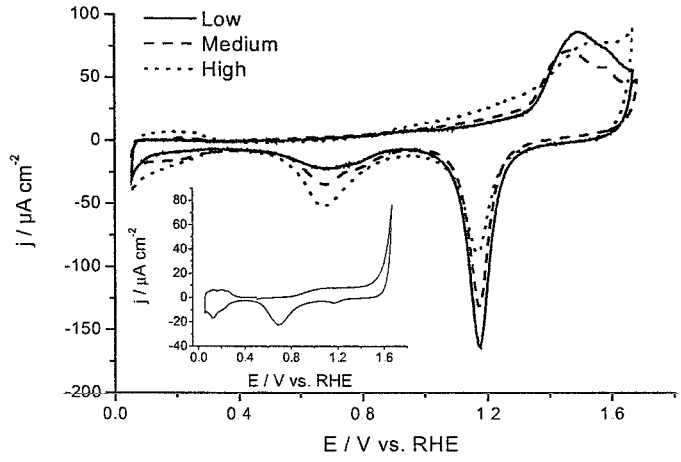

***Figure 3**. Blank cyclic voltammograms of the platinum modified gold surfaces in 0.5 M H_2SO_4.. The scan rate was 20 $mV \cdot s^{-1}$. The inset shows a CV of gold with a very high Pt concentration.*

0.67 V in the negative going scan. Oxidation and reduction of the gold surface occurs at 1.35 V in the positive going scan and 1.17 V in the negative going scan, respectively. As the platinum concentration is increased, the Pt oxidation/reduction charge increases while the gold oxide formation/reduction charge decreases, due to masking of the substrate surface. Similar results were obtained by Friedrich et al. in $HClO_4$ by depositing colloidal platinum particles on a gold substrate.[9] At high platinum concentrations the shape of the surface oxidation region starts to resemble that of polycrystalline Pt. (Depositing very large quantities of Pt produces CVs similar to those given by Möller et al.[21] for platinum-gold alloys (see the inset in Fig. 3).)

Friedrich et al. introduced a method for calculating the coverage of the gold supported platinum particles based on the real surface area of the gold electrode and the area of the Pt particles.[9] The real surface area of the gold electrode, A_{Au}^{0}, is easily determined by measuring the charge of the gold oxide reduction peak in a blank cyclic voltammogram recorded from 0.05 to 1.7 V vs. RHE at a scan rate of 20 $mV \cdot s^{-1}$, which forms a gold oxide layer that should have a charge of ca. 380 $\mu C \cdot cm^{-2}$.[22, 23] The determination of the Pt nanoparticle area is less straightforward as geometrical structure and the size dispersion of the particles is unknown. However, if the electrochemically active area (ECA) of the Pt particles is known, a coverage-analogous quantity, Γ_{Pt}, can be calculated using the real surface area of the gold electrode.

$$\Gamma_{Pt} = \frac{A_{Pt}}{A_{Au}^{0}} \qquad \text{(Eq. 1)}$$

An estimate of the ECA of the platinum particles can be determined from the Pt oxide reduction charge obtained from the BCVs of the Pt modified Au electrodes (recorded under the same conditions as suggested by Angerstein-Kozlowska et al.) and relating this value to the corresponding value found for polycrystalline Pt of 440

$\mu C \cdot cm^{-2}$.[24] The calculated coverages for the surfaces with "low", "medium" and "high" platinum concentrations are 0.28; 0.36 and 0.49, respectively.

As the AFM equipment requires relatively flat and smooth surfaces, the characterization of the nanoparticles was performed using gold plates supplied by Arrendee™ as substrate in the platinum deposition experiment. Prior to Pt deposition, the gold plates were flame annealed and carefully cooled down in an Argon gas stream. Although this procedure results in large atomically flat Au(111) planes, it otherwise does not affect the formation of the platinum particles, as is apparent from a comparison of the CVs of the thus generated samples to the CVs shown in Fig. 3.

The resulting AFM images for the low, medium and high platinum surface concentrations can be found in Fig. 4a,b and c, respectively. Fig. 4a shows the surface morphology of Pt-Au electrode with low Pt coverage (θ_{Pt}=0.28), and demonstrates the presence of particles with an average diameter of 10-20 nm. It is possible that smaller particles are also present on the surface, however, these cannot be detected due to the relatively low sensitivity of the AFM setup. At higher surface concentrations (see Fig. 4b and c) the particle size distribution increases to 10-120 nm for medium platinum concentrations and to platinum monolayers for high Pt concentrations.

Generally, the AFM images clearly show that platinum does not grow epitaxially but rather forms islands in the gold substrate in a Volmer-Weber type growth. For bi-metallic systems (in thermodynamic equilibrium), a Volmer-Weber growth mode is expected when the sum of the relative free surface energies (in this case $\Delta\gamma = \gamma_{Pt} + \gamma_{Au\text{-}Pt} - \gamma_{Au}$) of the pure metal ($\gamma_{Pt}$), the pure substrate ($\gamma_{Au}$) and the interface ($\gamma_{Au\text{-}Pt}$) is smaller than zero.[25-27]

3.3. Carbon Monoxide Oxidation

The effect of the platinum surface morphology on the electrooxidation of CO was investigated by CO adlayer stripping and bulk CO oxidation experiments.

3.3.1. Surface Stability

Fig. 5 demonstrates the effect of changes in the surface morphology induced by repetitive cycling to high potentials on the continuous oxidation of CO. Cycling up to 1.2 V vs. RHE results in a decrease of maximum current density for the oxidation of CO, which, in the absence of surface contamination, indicates a decrease in available platinum sites at the surface. This decrease in available Pt sites may be due to agglomeration of the platinum particles or embedding/alloying of Pt with the Au surface.[28] In order to reduce the influence of morphology changes on our experiments only a single scan up to 1.2 V is recorded for each measurement.

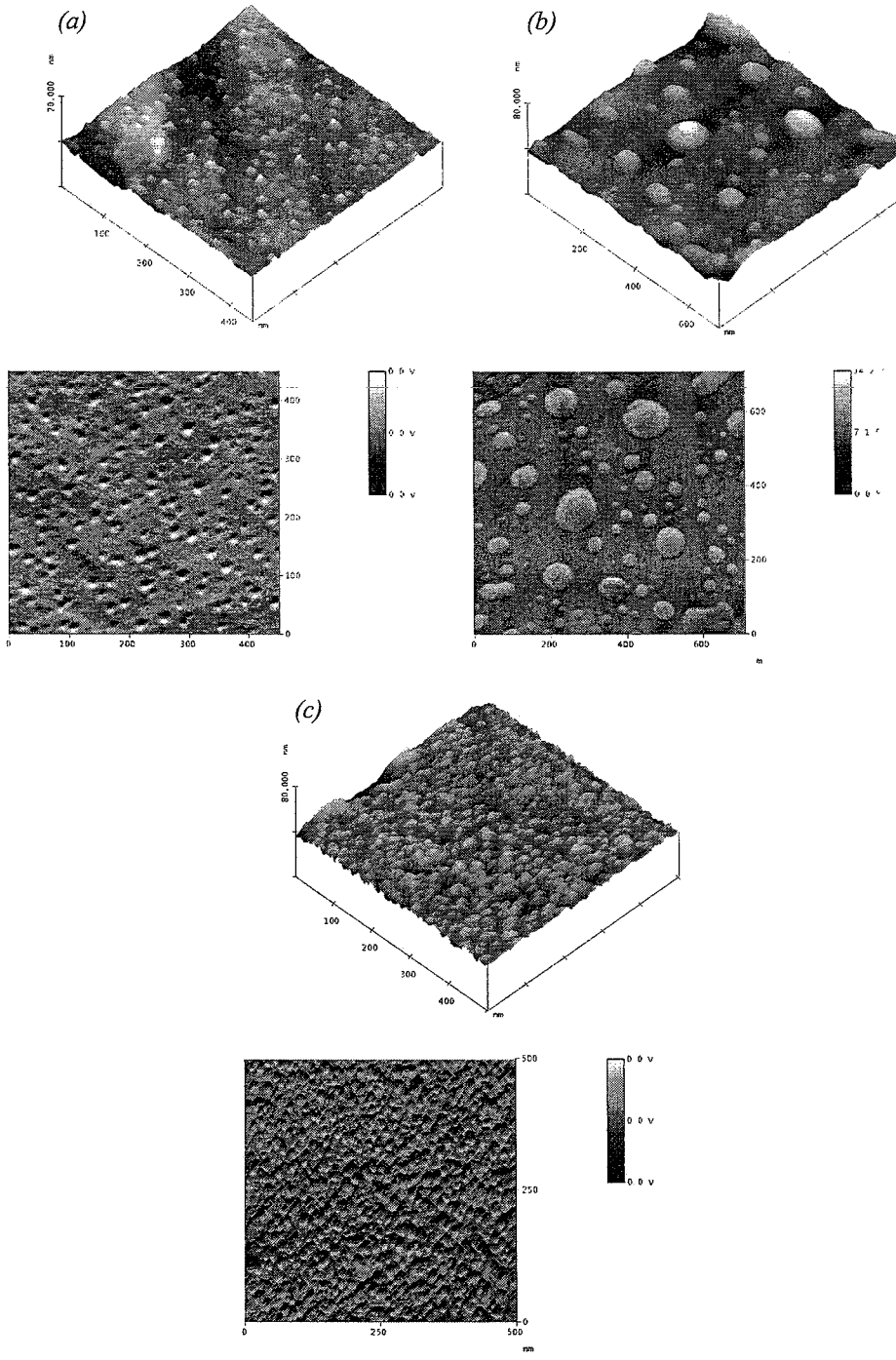

Figure 4. *Atomic force microscopy images of the Pt-Au surfaces, with a) low b) medium and c) high platinum concentrations*

Fig. 6 illustrates that the platinum deposition rate also influences the morphology of the particles, and, therefore, affects the electrooxidation reaction. The two surfaces investigated in Fig. 6 were generated by keeping the total deposition charge constant (5000 $\mu C \cdot cm^{-2}$, per geometrical surface area) but changing the ratio between the applied current and the deposition time. The surface resulting in the first curve (solid thin line) was generated by a current of 50 $\mu A \cdot cm^{-2}$ applied for 100 seconds, while the second surface (dashed line) was generated by 500 $\mu A \cdot cm^{-2}$ for 10 seconds. The figure clearly

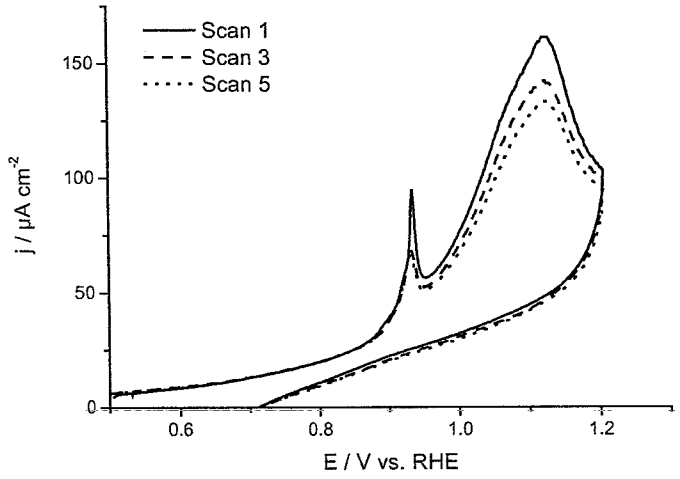

Figure 5. *Influence of repetitive cycling on the CO electrooxidation characteristics of a Pt-Au electrode with a "medium" Pt coverage recorded in a CO saturated solution of 0.5 M H2SO4 at 20 mV·s^{-1}.*

shows that increasing the Pt deposition rate results in a decrease in the CO oxidation potential. This effect, according to groups of Markoviç and Stimming, suggests a stronger particle size effect for surfaces generated by slow Pt deposition, i.e. the generated particles are assumed to be smaller in size.[9-11]

Interestingly, Arenz et al.[11] proposed that the oxidative stripping of CO is mainly controlled by the number of defect sites, which may serve as an active center for OH adsorption, rather than the mobility of CO. Using transmission electron microscopy (TEM), they found that decreasing the particle size leads to a concomitant decrease in the number of defects. Moreover, as it is well known that CO adsorbs and oxidizes preferentially at step sites,[29-31] the negative potential shift recorded on surface generated by rapid platinum deposition may also be ascribed to an increase in the number of surface defects.

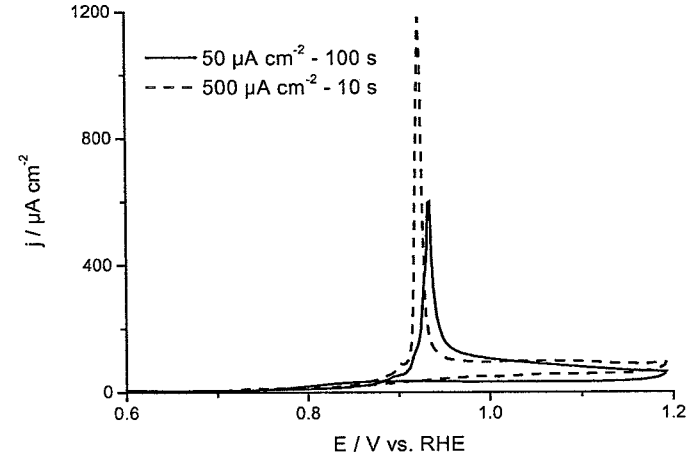

Figure 6. *Influence of the platinum deposition rate on the CO electrooxidation characteristics of a Pt modified Au electrode with a high Pt coverage recorded in 0.5 M H_2SO_4 at 20 mV·s^{-1}.*

3.3.2. Cyclic Voltammetry: Saturated CO-adlayer stripping

Fig 7 displays CO stripping CVs recorded on the Pt-Au electrodes at a scan rate of $20mV \cdot s^{-1}$. At low platinum coverages a peak is observed at 1.07 V vs. RHE. This feature remains as the platinum surface concentration is increased. On the Pt-Au electrode with 50-120 nm size particles another feature appears at 0.9 V vs. RHE appears, which becomes the dominant feature at high platinum coverages.

As our AFM analysis indicates that the particles on the low Pt-Au electrode are ca. 10-20 nm (or smaller) in diameter, we ascribe the peak located at 1.07 V to oxidative removal of CO adsorbed on these small particles. For the medium platinum surface concentrations, in addition to the 10-20 nm size particles, Pt particles with a diameter of ca. 50-120 nm were found, which we believe are responsible for the appearance of the second feature at 0.9 V vs. RHE. At even higher platinum coverages the surface displays oxidation characteristics typical for polycrystalline platinum surfaces,[32] which is in agreement with the presence of thick platinum layers (see Fig. 4c). Interestingly, Friedrich et al. also obtained similar CVs for agglomerates of well-defined colloidal nano-particles on gold. For particles with an average diameter of 3 nm, they observed a peak at 1.0 V vs. RHE (at coverages of $\theta_{Pt} = 0.05$ and $\theta_{Pt} = 0.24$). At $\theta_{Pt} = 0.39$ a second peak at 0.87 V vs. RHE was observed, which, as the CV displays polycrystalline platinum characteristics, was attributed to CO oxidizing on the nano-particle agglomerates. In addition, on small Pt nanoparticles with a mean particle size of 1.9 nm supported on glassy carbon, Maillard et al. also report a CO stripping peak at 0.99 V.

It is noteworthy that, although our particles are much larger than those used by Friedrich et al. and Maillard et al., the distinct "particle size effect" is still present. Thus suggesting that perhaps not the size of the particle matters, but rather the shape or morphology (as was also implied by Friedrich et al. and Arenz et al.[9, 11]). Furthermore, the fact that most of these studies were performed on well-defined particles,

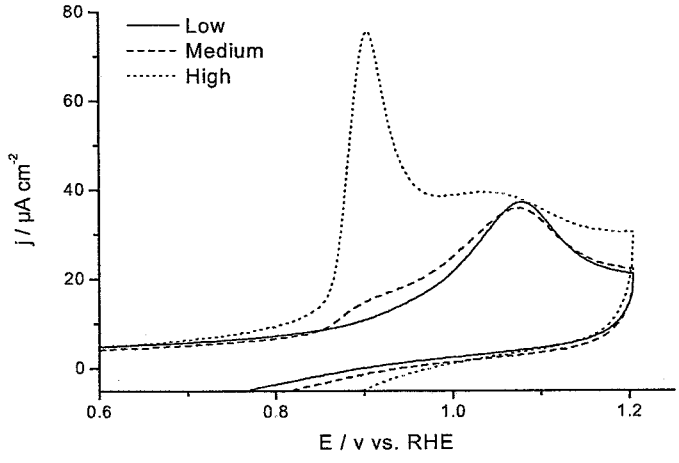

***Figure** 7. CO-adlayer stripping voltammograms on the Pt modified Au electrodes in 0.5 M H_2SO_4 at 20 $mV \cdot s^{-1}$.*

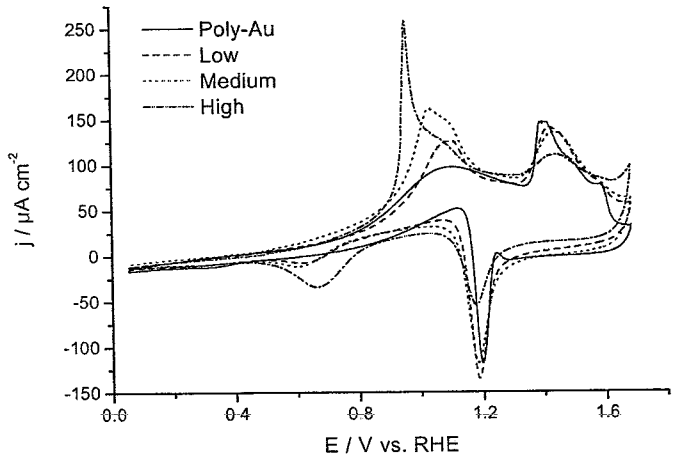

Figure 8. *Bulk CO oxidation voltammograms on bare gold and Pt modified Au electrodes in 0.5 M H_2SO_4 at 20 $mV \cdot s^{-1}$.*

while our particles are irregular in shape (and size) and yet both systems display the characteristic "particle size effect", also suggests that the size of the particles is not as important as is generally presumed.

3.3.3. Cyclic voltammetry: Bulk CO oxidation

Bulk CO oxidation experiments were performed in a CO saturated solution (bubbling CO for 15 minutes through the blank electrolyte). The obtained CO oxidation CVs on bare polycrystalline Au and the Pt-modified Au electrodes are presented in Fig. 8.

On polycrystalline Au CO oxidizes between ca. 0.8 V and 1.3 V vs. RHE, after which the formation of gold oxides inhibit the reaction. Due to continuous readsorption of CO from the electrolyte, the oxidation features recorded on the Pt-modified electrodes are shifted towards higher potentials compared to CO-adlayer stripping. This positive shift is well-known for Pt electrodes, and can be as high as 300 mV.[30, 32] In general, increasing the amount of Pt on the surface results in an overall increase of the current density, signifying a higher number of reactive sites. For the Pt-Au surface with 20-50 nm small particles an oxidation peak is observed at 1.1 V, which shifts to lower potentials as the particle size (and number of particles) is increased. At high Pt coverages, the main CO oxidation peak is located at 0.96 V. However, even at these high coverages the feature ascribed to oxidation on small particles is still visible at 1.1 V.

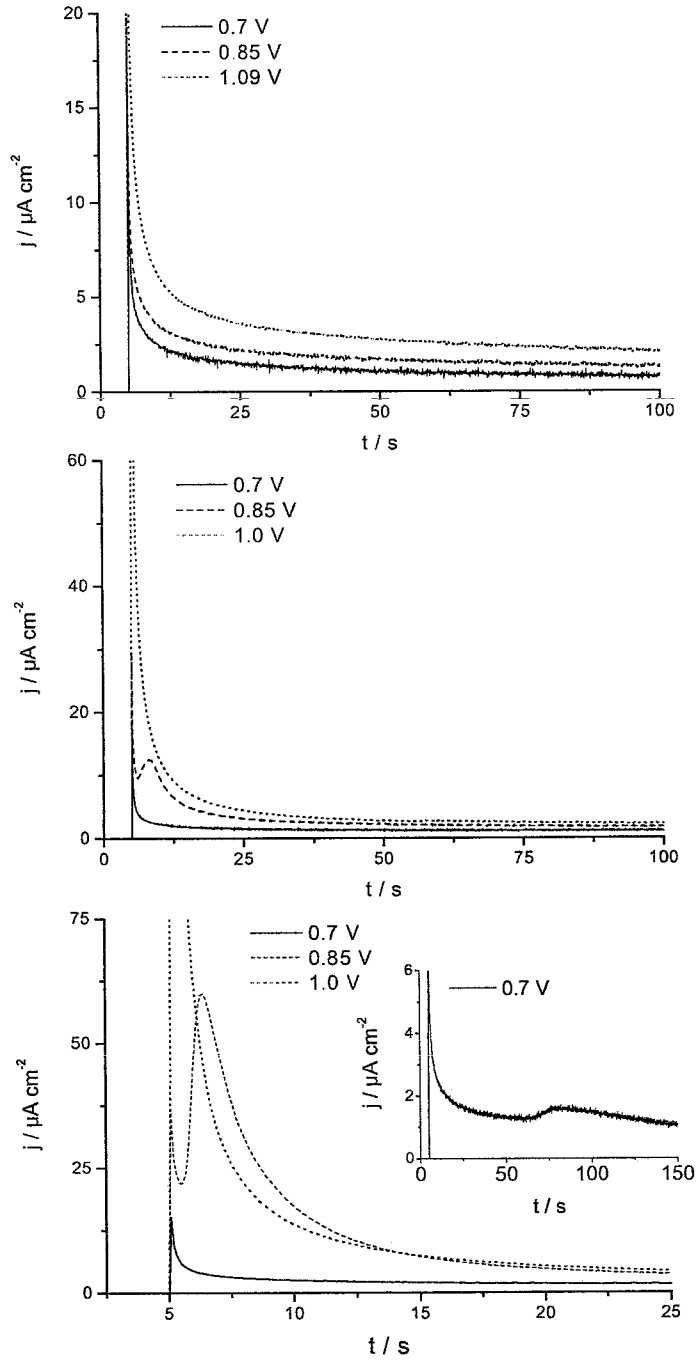

Figure 9. *Current-time transients for saturated CO adlayers on the three Pt-Au electrodes with (a) low, (b) medium and (c) high platinum coverage. Step potentials are listed in the figure. The inset in Fig 9.9c shows a zoom of the transient recorded at 0.7 V.*

3.3.4. Chronoamperometry

Potential-step experiments provided a more detailed picture of the kinetics of the CO oxidation reaction on the gold supported platinum nanoparticles. The final potentials under investigation were 0.7, 0.85 and 1 V vs. RHE. The resulting current-time curves for Au electrodes with low, medium and high Pt surface concentrations are shown in Fig. 9a-c, respectively. All the transients recorded on the surface with the low platinum

coverage display a current decay (see Fig. 9a), while the surfaces with medium and high Pt coverages show a peak in the transient recorded at 0.85 V (see Fig 9b and c). For the highest amount of platinum, a current maximum was also found at 0.7 V vs. RHE. At potentials higher than 1 V, all three electrodes display a current decay, which seems identical for each surface. Considering the relatively high final potential applied, the formation of oxides on the nanoparticles is the most likely cause of this decay.

Potential-step experiments performed by Friedrich et al. on nanoparticles of ca. 3 nm and agglomerates of these particles (ca. 16 nm in diameter), also showed a current decay on the small particles and a current maximum on the larger agglomerates.[9] Based on these results they concluded that the oxidation of CO on small particles follows an Eley-Rideal type mechanism, while a Langmuir-Hinshelwood type mechanism applies for the larger agglomerates. However, in contrast to these observations, Maillard et al. reported that chronoamperometric transients recorded on 1.9-3.1 nm size particles do in fact exhibit current maxima in the potential range under investigating, indicating that a Langmuir-Hinshelwood type mechanism seems more appropriate.[10]

From this perspective, it is puzzling that our ill-defined "small particles" (of 10-20 nm), which are even larger than the agglomerates used by Friedrich et al., display a current decrease rather than a current maximum. Perhaps the high size and shape dispersion of our particles leads to an overlap of the transient behavior of multiple morphologies and, thus, in an overall decaying transient. More research is needed to clarify these findings.

3.3.5. Surface Enhanced Raman Spectroscopy

Fig. 10 shows SER spectra of the Au-Pt (medium coverage) electrode in sulfuric acid saturated with CO at different potentials. Two spectral regions are found to exhibit some important changes, as the potential is made more positive. One, at low frequencies ranges (Fig. 10a), show tree bands. The band centered at 380 cm^{-1} can be assigned as stretching mode of CO adsorbed on a platinum bridge site, this mode blue shifts with a Stark tuning rate of -12cm^{-1}/V. The band at 460 cm^{-1} corresponds to the stretch mode of atop CO adsorbed on platinum,[33-35] and has a Stark tuning of –16 cm^{-1}/V. Both modes disappear at potential higher than 1 V for medium platinum coverage. A band centered around 580 cm^{-1} appears as the potential exceeds 1.3 V, coinciding with the Au surface reduction peak in the voltammogram. Weaver et al. attributed this band, which has a small but significant positive Stark tuning slope (ca. 10 cm^{-1}/V), to the combined vibrations of Au-O and Au-OH surface species.[36, 37] Other authors have also concluded, on the basis of other techniques, that the layer formed on gold above 1.2 V is composed of both surface oxide and surface hydroxide.[38, 39] But Tian's group observed a band at 570 cm^{-1} on a pure platinum substrate,[34] and Weaver's group a similar band on a platinum film on gold.[35] Both attributed the band to the Pt-O bond. Unfortunately, differentiation of these three surface species is not straightforward.

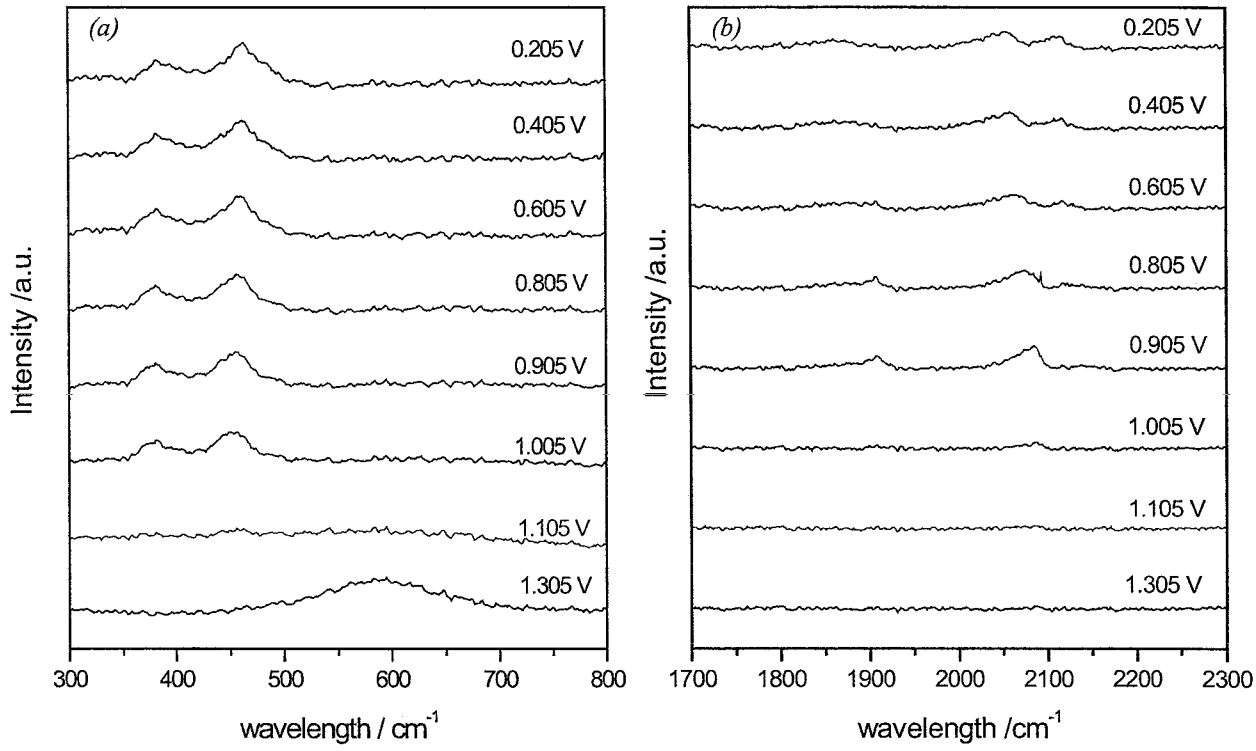

***Figure 10**: Low (a) and high frequency range (b) SER spectra obtained for a Au-Pt (Medium) electrode in 0.5 M H_2SO_4 at the indicated potentials.*

A second spectral region is defined by the 1700-2300 cm^{-1} window (Fig. 10b), with three peaks. The band at 1890cm^{-1} could be attributed to the CO stretching mode on platinum bridge site,[34, 35, 40] with a Stark tuning slope of 40 cm^{-1}/V, this band is not detectable for high platinum covered gold electrode. A second band at 2050 cm^{-1} can be assigned to the atop CO on platinum [33-37, 40] and it shows a Stark tuning of 50cm^{-1}/V. A third band at 2120cm^{-1} is observed, ascribable to the stretching frequency of CO adsorbed atop on gold, these band red shifts, and the approximate Stark tuning slope of 40 cm^{-1}/V.[40, 41]

These bands are all observed in the three different platinum covered surfaces and display similar characteristics, the CO bands are presents at potential negative with respect to the oxidation peak in the voltammograms. The intensity of these bands is almost constant if they involve Pt-CO bonds, but in the case of the Au-CO mode are decreasing at more positive potentials analogous to the oxidation of CO on pure gold electrodes.[42] The band involving OH species in the surface (590 cm^{-1} band) is only present at more positive potentials.

3.4. Methanol and Formic Acid Oxidation

The effect of particle size and morphology was also studied for the oxidation of methanol and formic acid, using cyclic voltammetry and chronoamperometry.

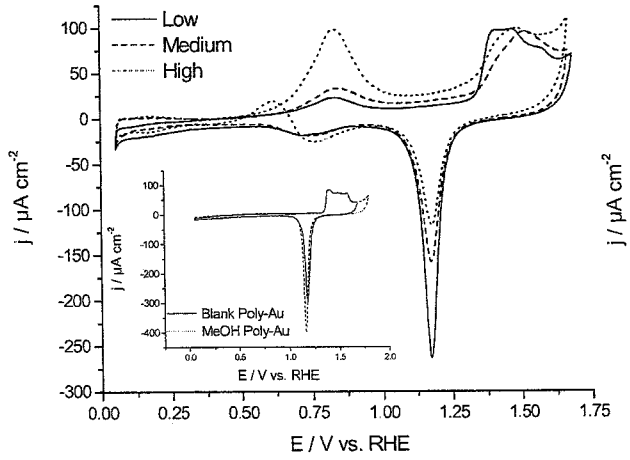

Figure 11. *Cyclic voltammograms of the methanol oxidation on the three Pt modified Au surface in 0.5 M H_2SO_4 at 20 $mV \cdot s^{-1}$.*

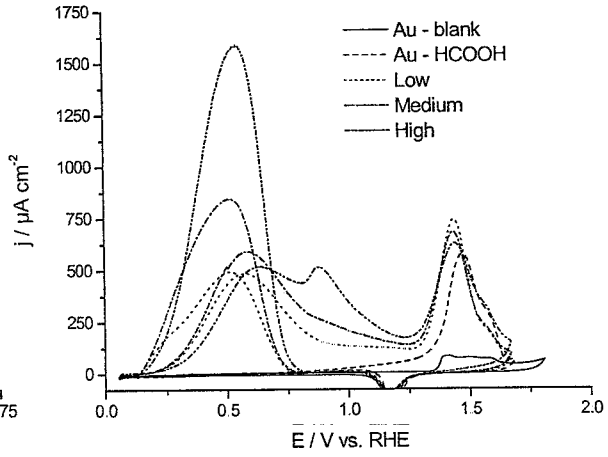

Figure 12. *Cyclic voltammograms of the formic acid oxidation on the three Pt modified Au surfaces in 0.5 M H_2SO_4 at 20 $mV \cdot s^{-1}$.*

3.4.1. Cyclic Voltammetry

The CVs for the methanol and formic acid oxidation on the Pt-Au electrodes can be found in Fig. 11 and 12, respectively. The inset in Fig. 11 demonstrates that bare gold is virtually inactive towards the oxidation of methanol. However, deposition of even a small amount of Pt on the gold surface immediately leads to the appearance of a peak at 0.84 V vs. RHE. As the amount of Pt is increased the total charge of the MeOH oxidation peak increases, while the onset of the reaction decreases from 0.65 V to 0.6 V and 0.55 V when going from low to medium and high Pt concentrations, respectively.

While gold is inactive towards the oxidation of methanol, it can oxidize formic acid at sufficiently high potentials, especially in the absence of strongly adsorbing anions (see Fig. 12).[43-46] The onset of the HCOOH oxidation on polished gold electrodes lies at ca. 0.8 V. Deposition of small amounts of platinum results in the appearance of an oxidation peak at 0.58 V vs. RHE in the positive going scan, which shifts to more positive potentials as the platinum coverage is increased. At high platinum coverages a second feature at 0.89 V becomes visible. A similar feature was also observed for polycrystalline platinum electrodes, which leads us to conclude that this peak is most likely due to oxidation of formic acid on large particles and platinum overlayers.[47] The peak at 0.58 V can be ascribed to the oxidation of HCOOH to CO_2 on Pt sites, which are unblocked by preadsorbed poisoning species like CO.[47, 48] Compared to polycrystalline gold, the onset of the formic acid oxidation on Pt modified Au electrodes is shifted to considerably more negative potentials (at ca. 0.2 V vs. RHE).[47] In the negative going scan, the reaction proceeds on a surface, which has been oxidatively stripped of preadsorbed blocking species, thus higher current densities are obtained.

In order to compare the methanol and formic acid oxidation activities of the platinum modified surfaces, the CVs were normalized for the amount of platinum deposited, which was estimated by integration of the Pt oxide reduction peak. The resulting graphs are presented in Fig. 13 and 14a and b. Although the platinum oxide

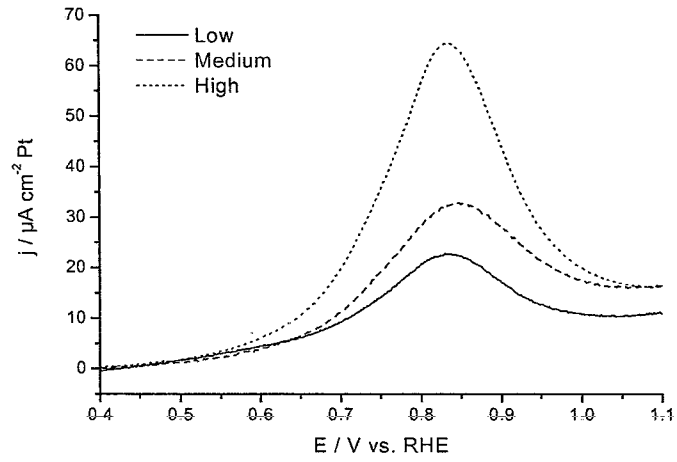

Figure 13. *Cyclic voltammograms of the methanol oxidation activity for the different Pt concentrations, normalized for the amount of Pt in 0.5 M H_2SO_4 at 20 mV·s^{-1}.*

reduction charge is only a rough estimate of the total platinum coverage, Fig. 13 clearly shows that larger Pt particles are more active towards the methanol oxidation than smaller particles (of equal active surface area). Apparently, the oxidation of methanol suffers from the same particle size effect as carbon monoxide. Fig. 14a and b shows similarly corrected plots for the oxidation of HCOOH in the positive and negative going scan, respectively. In the positive going scan the current density is highest for the surface with the lowest Pt coverage. As the amount of platinum is increased, the current maximum decreases, which implies that smaller particles are more active towards formic acid oxidation than larger polycrystalline-like structures. It is also likely that surface poisoning plays an important role on the large particles. In the return scan, however, the oxidation activity increases with the amount of platinum deposited. As the potential decreases below 0.3 V the order of the oxidation activity is again inverted, with the low Pt-Au surface now being more active than the higher coverages. These results suggest

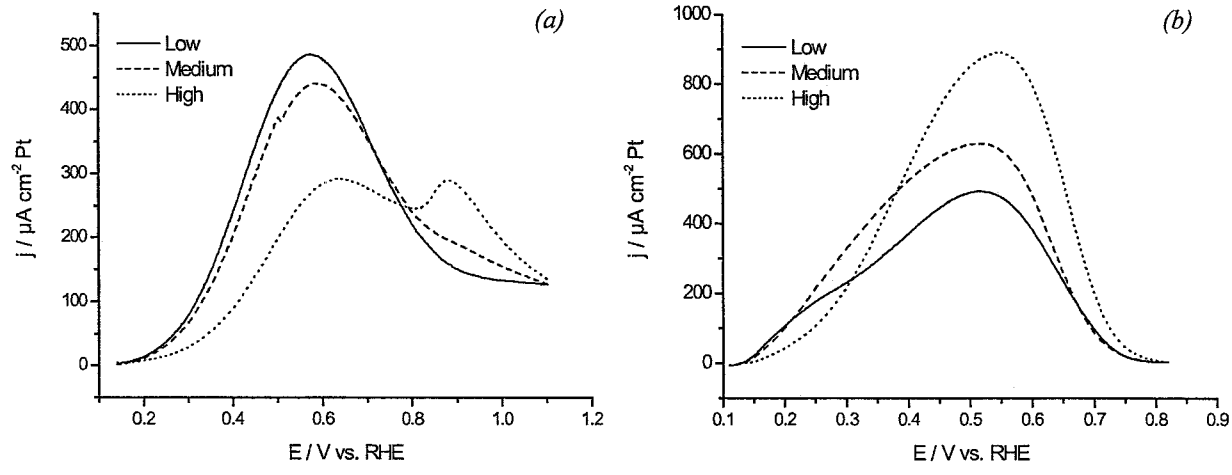

Figure 14. *Cyclic voltammograms of the formic acid oxidation activity for the different Pt concentrations, normalized for the amount of Pt, with a) the positive going scan and b) the negative scan in 0.5 M H_2SO_4 at 20 mV·s^{-1}.*

that larger particles are more active towards the oxidation of formic acid, but also poison faster.

Park et al.[8] explained the decreasing methanol reaction rate for a decreasing particle size by a loss of adjacent available Pt terrace sites on nanoparticles smaller than 4 nm in diameter. They suggested that the dissociation of methanol to reactive intermediates and chemisorbed CO requires an ensemble of catalytically active terrace sites. Thus, the decreasing oxidation activity for decreasing particle size can be attributed to a drop in the number of Pt "ensemble sites" available to the adsorption and decomposition of methanol. The fact that we can still observe an effect of the particle morphology on the reaction characteristics even for with a diameter up to ca. 120 nm, again suggests that the shape and morphology, rather than actual particle size play a predominant role in the reaction kinetics.

Interestingly, from a study of the MeOH oxidation reaction on stepped platinum electrodes of [n(111)×(111)] orientation, we concluded that methanol preferably decomposes on step sites rather than terrace sites.[49] Although these findings seem to contradict to those of Park et al.,[8] the OLEMS results show that the Pt(110) surface is less active towards methanol oxidation than the stepped surfaces Pt(554) and Pt(553) (of [(n-1)(111)×(110)] orientation).[50] Based on these results, we suggested that sites with both a step and terrace site may be particularly favorable "ensemble sites" for dissociative adsorption of methanol. This theory may be used to explain why particles larger than 3-4 nm in diameter can still display a pronounced "particle size effect". If the particles contain a large number of defects and relatively few contiguous terrace sites, the methanol oxidation rate may be lower due to formation of soluble intermediates. Such a situation is apparently easily satisfied on well-defined particles with an average diameter of ca. 2-5 nm,[6, 8-11, 51] but may also apply to our larger irregularly shaped structures. Moreover, the presence of defects may decrease the overall surface mobility of CO, thus enhancing the particle shape effect. Therefore, in agreement with other authors, we conclude that the particle shape indeed seems more important than the actual particle size.[9, 11] As formic acid does not require an ensemble of platinum sites, the reaction rate is found to increases for decreasing particle size (and, thus, increasing number of defects).

3.4.2. Chronoamperometry

The kinetics of the methanol and formic acid oxidation on nanoparticles generated for medium coverages, were also investigated using potential-step experiments. The steady-state current recorded at 300 seconds (obtained analogous to ref. [49]) was found to follow the shape and position of the oxidation peak recorded in the cyclic voltammetry. The current densities recorded in the methanol as well as the formic acid containing electrolyte were found to increase with the potential (with maxima at 0.8 and 0.6 V vs. RHE for MeOH and HCOOH, respectively) until the onset of surface oxidation, after which the current decreases again. As the obtained graphs do not provide

any new information in addition to those presented in ref. [49], the corresponding graphs are not presented in this report.

4. Conclusion

The electrooxidation characteristics of carbon monoxide, methanol and formic acid on Pt particles of varying size were investigated by voltammetry and chronoamperometry. The particles were generated by galvanostatic deposition of platinum on polished polycrystalline gold electrodes. Three surfaces of low, medium and high Pt surface coverage were generated by galvanostatic deposition of platinum on polished polycrystalline gold electrodes and characterized by voltammetry and an Atomic Force Microscopy analysis. The electrodes with low and medium platinum coverages consisted of small ill-defined particles with diameters ranging from 10-20 and 10-120 nm, respectively. At higher platinum coverages Pt overlayers are formed.

Based on CO stripping voltammetry and bulk CO oxidation experiments we can conclude the following:

1. CO stripping and bulk CO oxidation experiments on irregularly shaped particles with an average diameter of 10-20 nm display a pronounced particle size effect, while Friedrich et al. observe polycrystalline platinum like oxidation characteristics for 16nm large agglomerates of well-ordered particles.[52] Therefore, we conclude that not the size, but the shape of the particles is crucial to the oxidation characteristics.
2. Current-time transients recorded on these small 10-20 nm size particles showed a current decay, which can be explained by assuming an Eley-Rideal type reaction mechanism, or by assuming that overlapping signals of a Langmuir-Hinshelwood type reaction on particles of varying size produce an overall current decay. On lager particles a Langmuir-Hinshelwood type mechanism is found.
3. Surface Enhanced Raman Spectroscopy experiments indicated a difference in the ratio between CO bonded linearly and in bridge configuration on the small, medium and large Pt nano-particles, again indicating the dominant role of the surface morphology, rather than particle size.
4. The oxidation activity of methanol was found to decrease with the particle size, while the formic acid oxidation rate increases. Again a "particle size effect" is observed for nanoparticles of ca. 120 nm in diameter, which is much larger than the particles for which a particle size effect is reported in the literature. This emphasizes the previously made suggestion that "particle size" is not as important as particle shape. The particle shape effect for the methanol oxidation reaction can be explained by a reduction in available "ensemble sites" and a reduction in the mobility of CO formed by decomposition of methanol. As formic acid does not require Pt ensemble sites decreasing the particle size, and thus, the relative number of defects, increases the reaction rate.

In general, based on our results, we conclude that the "particle size effect", reported in the literature should be critically reviewed. A "particle shape effect" in many cases may be a more appropriate term.

Acknowledgement: This research was supported by the Netherlands Foundation for Scientific Research (NWO).

References

[1] M. S. Wilson, F. H. Garzon, K. E. Sickafus, and S. Gottesfeld, J. Electrochem. Soc. 140 (1993) 2872.
[2] R. Parsons and T. VanderNoot, J. Electroanal. Chem. 257 (1988) 9.
[3] M. L. Sattler and P. N. Ross, Ultramicroscopy 20 (1986) 21.
[4] L. J. Bregoli, Electrochim. Acta. 23 (1978) 489.
[5] Y. Takasu, N. Ohashi, X. G. Zhang, Y. Murakami, H. Minagawa, S. Sato, and K. Yahikozawa, Electrochim. Acta. 41 (1996) 2595.
[6] T. Frelink, W. Visscher, and J. A. R. van Veen, J. Electroanal. Chem. 382 (1995) 65.
[7] O. V. Cherstiouk, P. A. Simonov, and E. R. Savinova, Electrochim. Acta. 48 (2003) 3851.
[8] S. Park, Y. Xie, and M. J. Weaver, Langmuir 18 (2002) 5792.
[9] K. A. Friedrich, F. Henglein, U. Stimming, and W. Unkauf, Electrochim. Acta. 45 (2000) 3283.
[10] F. Maillard, M. Eikerling, O. V. Cherstiouk, S. Schreier, E. Savinova, and U. Stimming, Faraday Discuss. 125 (2003) 357.
[11] M. Arenz, K. J. J. Mayrhofer, V. Stamenkovic, B. B. Blizanac, T. Tomoyuki, P. N. Ross, and N. M. Markovic, J. Am. Chem. Soc. (2005) submitted.
[12] N. M. Markovic and P. N. Ross, Surf. Sci. Rep. 45 (2002) 117.
[13] T. Iwasita, Electrochim. Acta. 47 (2002) 3663.
[14] A. Hamnett, Comp. Chem. Kin. (1999) 635.
[15] T. D. Jarvi, S. Sriramulu, and E. M. Stuve, J. Phys. Chem. B 101 (1997) 3649.
[16] M. Shibata and S. Motoo, J. Electroanal. Chem. 209 (1986) 151.
[17] H. Wang, C. Wingender, H. Baltruschat, M. Lopez, and M. T. Reetz, J. Electroanal. Chem. 509 (2001) 163.
[18] H. Wang, T. Loffler, and H. Baltruschat, J. Appl. Electrochem. 31 (2001) 759.
[19] K.-I. Ota, Y. Nakagawa, and M. Takahashi, J. Electroanal. Chem. 179 (1984) 179.
[20] P. Gao, D. Gosztola, L. W. H. Leung, and M. J. Weaver, J. Electroanal. Chem. 233 (1987) 211.
[21] H. Möller and P. C. Pistorius, J. Electroanal. Chem. 570 (2004) 243.
[22] H. Angerstein-Kozlowska, B. E. Conway, A. Hamelin, and L. Stoicoviciu, Electrochim. Acta. 31 (1986) 1051.
[23] H. Angerstein-Kozlowska, B. E. Conway, A. Hamelin, and L. Stoicoviciu, J. Electroanal. Chem. Inter. Electrochem. 228 (1987) 429.
[24] D. V. Heyd and D. A. Harrington, J. Electroanal. Chem. 335 (1992) 19.
[25] E. Bauer, Z. Krist. 110 (1958) 395.
[26] E. Bauer and J. H. Van der Merwe, Phys. Rev. B 33 (1986) 3657.
[27] A. Zangwill, Physics at Surfaces, Cambridge Univ. Press, Cambridge, 1988.
[28] M. O. Pedersen, S. Helveg, A. Ruban, I. Stensgaard, E. Laegsgaard, J. K. Norskov, and F. Besenbacher, Surf. Sci. 426 (1999) 395.
[29] N. P. Lebedeva, M. T. M. Koper, J. M. Feliu, and R. A. van Santen, Electrochem.Commun. 2 (2000) 487.
[30] N. P. Lebedeva, M. T. M. Koper, E. Herrero, J. M. Feliu, and R. A. van Santen, J. Electroanal. Chem. 487 (2000) 37.
[31] N. P. Lebedeva, M. T. M. Koper, J. M. Feliu, and R. A. van Santen, J. Phys. Chem. 106 (2002) 12938.
[32] H. A. Gasteiger, N. M. Markovic, and P. N. Ross, Jr., J. Phys. Chem. 99 (1995) 8290.
[33] J. L. Gland and E. B. Kollin, Surf. Sci. 151 (1985) 260.

[34] Z. Q. Tian, B. Ren, and B. W. Mao, J. Phys. Chem. B 101 (1997) 1338.
[35] L. W. H. Leung and M. J. Weaver, J. Am. Chem. Soc. 109 (1987) 5113.
[36] J. Desilvestro and M. J. Weaver, J. Electroanal. Chem. Interfacial Electrochem. 209 (1986) 377.
[37] Y. Zhang, X. Gao, and M. J. Weaver, J. Phys. Chem. 97 (1993) 8656.
[38] G. Tremiliosi-Filho, L. H. Dall'Antonia, and G. Jerkiewicz, J. Electroanal. Chem. 422 (1997) 149.
[39] S. J. Xia and V. I. Birss, J. Electroanal. Chem. 500 (2001) 562.
[40] S. Zou, C. T. Williams, E. K. Y. Chen, and M. J. Weaver, J. Am. Chem. Soc. 120 (1998) 3811.
[41] G. L. Beltramo, T. E. Shubina, and M. T. M. Koper, PhysChemPhys In press (2005)
[42] M. A. Tadayyoni and M. J. Weaver, Langmuir 2 (1986) 179.
[43] G. Crepy, C. Lamy, and S. Maximovitch, J. Electroanal. Chem. 54 (1974) 161.
[44] A. Hamelin, Y. Ho, S. C. Chang, X. Gao, and M. J. Weaver, Langmuir 8 (1992) 975.
[45] Y. Zhang and M. J. Weaver, Langmuir 9 (1993) 1397.
[46] S.-l. Chen, B.-l. Wu, and C.-s. Cha, J. Electroanal. Chem. 431 (1997) 243.
[47] G.-Q. Lu, A. Crown, and A. Wieckowski, J. Phys. Chem. B 103 (1999) 9700.
[48] A. Capon and R. Parsons, J. Electroanal. Chem. 44 (1973) 239.
[49] T. H. M. Housmans and M. T. M. Koper, J. Phys. Chem. B 107 (2003) 8557.
[50] T. H. M. Housmans, A. H. Wonders, and M. T. M. Koper, J. Am. Chem. Soc. submitted (2005)
[51] O. V. Cherstiouk, P. A. Simonov, V. I. Zaikovskii, and E. R. Savinova, J. Electroanal. Chem. 554-555 (2003) 241.
[52] K. A. Friedrich, F. Henglein, U. Stimming, and W. Unkauf, Colloids and Surfaces, A: Physicochemical and Engineering Aspects 134 (1998) 193.